Cell cycle arrest following pan-RAS inhibition can occur through upregulation of p27 in both KRAS-dependent and KRAS-independent colon cancer cell lines

Caleb K. Stubbs, Marco Biancucci*, Vania Vidimar, Karla J. F. Satchell†

Department of Microbiology and Immunology, Northwestern University, Feinberg School of Medicine, Chicago, Illinois.

*Present address: GSK Vaccines, Rockville, MD 20850, USA.

†Corresponding author: Karla Satchell, Northwestern University, Feinberg School of Medicine, Chicago, IL 60611, USA. Email: k-satchell@northwestern.edu

ABSTRACT

RAS is one of the most frequently mutated oncogenes in cancer with ~30% of all human tumors harboring a mutation in either HRAS, NRAS, or KRAS isoforms. Despite countless efforts for development of small molecule inhibitors for RAS, it remains an elusive target in the clinic. Here we demonstrated that the pan-RAS biological inhibitor RAS/RAP1-specific endopeptidase (RRSP) has proteolytic activity in 'Ras-less' mouse embryonic fibroblasts expressing human RAS isoforms (H/N/KRAS) or major oncogenic KRAS mutants (G12C, G12V, G12D, G13D, and Q61R). The cleavage of RAS inhibited phosphorylation of ERK and cell proliferation. To investigate how RAS processing affects colon cancer cells, we tested RRSP against KRAS-dependent (SW620 and GP5d) and KRAS-independent (HCT-116, SW1463, and HT-29) cell lines and found that RRSP inhibited growth. The cleavage of RAS was cytotoxic in some cell lines and induced either irreversible cell cycle arrest or uncharacterized growth inhibition in others. The G1 cell cycle arrest in some colon cancer cells was mediated through rescue of p27 (Kip1) protein expression resulting in reduced phosphorylation of retinoblastoma protein. Together, this work demonstrated that complete ablation of RAS in cells induces growth inhibition, but the mechanism of inhibition can vary in different tumor cell lines. This ability of RAS processing to halt cell proliferation by multiple strategies highlights RRSP both as a potential anti-tumor therapy and as a tool for studying RAS signaling across tumor types.

Introduction

Thirty percent of all human cancers contain mutations in the proto-oncogene *RAS* that encodes a ~21 kDa small GTPase enzyme. The Ras sarcoma (RAS) GTPase cycles between GTP-bound (active) and GDP-bound (inactive) states for activation of downstream effectors, each playing key roles in cell proliferation and survival (1). This process is highly reliant on GTPase activating proteins (GAPs) and guanine exchange factors (GEFs) for hydrolysis of GTP and nucleotide exchange of GDP to GTP, respectively (2, 3). Nearly all RAS mutations occur as point mutations at Gly-12, Gly-13 or Gln-61, which disrupt GAP and/or GEF binding resulting in constitutive activation of RAS (1). Mutations in *RAS,* paired with loss of function in tumor suppressor genes, such as *TP53* and *APC*, are sufficient to fully transform cells and drive tumorigenesis (4). Among the major *RAS* isoforms (*HRAS*, *NRAS*, and *KRAS*), *KRAS* is the most frequently mutated isoform among all cancers (85%) followed by *NRAS* (11%) and *HRAS* (4%) (4). *RAS* mutations are highly enriched specifically in three of the four most lethal cancers in the United States, including pancreatic adenocarcinoma (98%), colorectal adenocarcinoma (52%), and lung adenocarcinoma (32%) (1, 4).

Upon growth receptor stimulation, the RAS protein recruits downstream effectors, including Rapidly Accelerated Fibrosarcoma kinase (RAF) and phosphatidylinositol-3-kinase. These effectors subsequently activate signaling pathways responsible for cell growth and survival, including the mitogen-activated kinase (MEK) to extracellular signal-regulated kinase (ERK) signaling pathway and the protein kinase B (also known as AKT) to mammalian target of rapamycin (mTOR) pathway, respectively (5, 6). RAS also regulates critical components involved in cell cycle. RAS activation is directly linked to hyper-phosphorylation of retinoblastoma protein (RB), thereby relieving its repression of E2F transcription factors, allowing transcription of G1 promoting genes, and promoting the cell cycle to progress from G1 to S phase (7).

Mechanisms that link RAS and the cell cycle have been well examined. In quiescent cells, the tumor suppressor p27 protein (also known as Kip1) is highly expressed in order to inhibit

cyclin-dependent kinase (CDK) activity and to suppress RB phosphorylation (8, 9). Upon mitogen stimulation, RAS activation suppresses p27 protein expression through post-translational modifications that signal for its ubiquitin-mediated degradation (10-12). In RAS-driven human cancers, low levels of p27 are frequently observed. This loss of p27 correlates with increased aggressiveness and poorer clinical outcomes in patients (13-18). Identifying strategies to restore expression of p27 could be effective to slow growth of RAS-driven cancers and lead to better overall survival in patients suffering from unregulated RAS signaling.

Although numerous studies support the advantages of targeting RAS to treat cancer, it remains an unsolved challenge in the clinic (19-23). Recent studies have taken advantage of biochemical properties of specific RAS mutants to develop selective small molecule inhibitors specific for highly oncogenic mutant forms of RAS. In particular, small molecules targeting KRAS G12C have been developed and are undergoing clinical trials (24-26). Despite this success, the strategy of selective inhibition has problems of being applicable to only a limited range of cancers integrated with personalized medicine and cannot be used to treat cancers that lack the specific mutation. To address this gap, new approaches are being developed to more broadly target RAS using biological proteases that cleave RAS (27, 28) or that target RAS for degradation (29).

Our lab has identified a potent protease that cleaves RAS called the Ras/Rap1-specific endopeptidase (RRSP). RRSP is a small domain of a large toxin secreted by the bacterium *Vibrio vulnificus* during host infection. *V. vulnificus* delivers RRSP into intestinal epithelial cells during host infection, where it targets all RAS isoforms and close homolog Ras-related protein 1 (RAP1). Through RAS inactivation, this bacterium suppresses the host immune response, thereby aiding systemic dissemination of the bacterium (30, 31). Detailed structural and biochemical studies have shown that RRSP attacks the peptide bond between Tyr-32 and Asp-33 in the Switch I region of both RAS and RAP1 (32). As a result, RAS and RAP1 are unable to undergo GTP-GDP exchange or bind to their downstream effectors (33, 34). Recently, RRSP engineered for *in vivo* delivery was shown to significantly reduce breast and colon tumor growth in xenograft mouse

models (27). The potential applicability of RRSP to a broad range of cancers was also tested using the standardized National Cancer Institute (NCI) cancer cell panel (35). Fourteen of 60 cell lines were classified as highly susceptible, 38/60 as susceptible, and only 8/60 showed low or no susceptibility to RRSP (27). The relative susceptibility of the cancer cells to RRSP did not correlate with any specific RAS mutation.

Distinct cancers vary in their dependency on mutant RAS for proliferation and survival. In cancer cell lines reliant on mutant KRAS, silencing of KRAS expression decreases signaling and activates caspase-dependent apoptosis, resulting in cell death (36). In other cancer cell lines, KRAS activity is dispensable and genetic silencing only modestly reduces ERK phosphorylation with no change in cell survival. A major impact of the discovery of RRSP as a protease that cleaves all isoforms of RAS is its utility to study the impact of pan-RAS inhibition on downstream signaling. Here, we investigate the downstream effect of RRSP processing of RAS on cell lines previously characterized as KRAS-dependent ($KRAS^{Dep}$) and KRAS-independent ($KRAS^{Indep}$) and the impact of RAS inhibition on cell growth and survival. We find that proteolytic processing of all isoforms of RAS is indeed a broadly applicable inhibitor. We demonstrate RRSP disrupts colon cancer cell growth through multiple mechanisms. In some cell lines, RRSP is cytotoxic, whereas in others, it induces a p27-dependent G1 cell cycle arrest. This study in total demonstrates that pan-RAS inhibition can be used across many cancers as a potential therapeutic and RRSP in particular can inhibit cell growth independent of KRAS mutation or KRAS-dependency.

Results

RRSP cleaves and inhibits proliferation in RAS wildtype and KRAS mutants cells

RRSP was previously shown to cleave KRAS G12D, G13D, and Q61R protein *in vitro* and to cleave KRAS G13D mutant protein within cells (32). To get a broader sense of the effectiveness of RRSP across different variants of oncogenic RAS, we tested RRSP against the 'RAS-less' MEF cell line panel developed by Drosten et al. (6). These cells have endogenous *RAS* genetically

deleted from their genome and replaced with a single allelic copy of human *RAS* gene. For delivery of RRSP into mouse cells, we used the anthrax toxin-based delivery system wherein the anthrax toxin lethal factor N-terminus was fused with RRSP (LF_NRRSP) or LF_NRRSP with a catalytically inactivating H4030A amino acid substitution (LF_NRRSP*). Intracellular delivery of RRSP (previously known as DUF5) with this system has been previously been demonstrated in several mammalian and mouse cell lines (32, 37, 39).

In MEFs expressing human KRAS, HRAS, or NRAS, treatment with 3 nM LF_NRRSP dramatically decreased intact full-length RAS levels with increased detection of cleaved RAS. For each isoform, LF_NRRSP was found to cleave at least 80% of RAS after 24 hours (**Fig. 1A)**. As expected, controls treated with PA alone or in combination with catalytically inactive LF_NRRSP* showed no change of intact RAS protein levels **(Fig. 1A and 1B).** We also observed similarities of RRSP activity in MEF cell lines expressing oncogenic KRAS, including G12V, G12D, G12C, G13D, and Q61R. Amongst each of the mutants RAS alleles tested, we observed ~25% of total RAS remaining following LF_NRRSP treatment with no significant loss of RAS in cells treated with PA (**Fig. 1B).** The oncogenic RAS variants with the higher percentage of RAS remaining following LF_NRRSP treatment were G13D, G12C and Q61R, although these differences were not statistically significant. Further, the total RAS remaining in each LF_NRRSP-treated MEF cell line was not statistically significant between groups.

In addition to cleavage of RAS, RRSP treated cells showed significant decreases in phosphorylation of ERK when compared to cells treated with PA alone or with the catalytically inactive LF_NRRSP* (**Fig. 1C and D)**. These data demonstrate that RRSP is equally effective in cells at cleaving all major wildtype RAS isoforms and all KRAS mutant isoforms tested resulting in reduced levels of pERK.

To test the impact of processing of different RAS isoforms on cell proliferation, 'RAS-less' mouse embryonic fibroblast (MEF) cells were treated with PA alone or in combination with LF_NRRSP or catalytically inactive LF_NRRSP* were tracked using time lapse imaging for four days.

At early timepoints following treatment, LF_NRRSP-induced a severe cell rounding that was not observed in PA alone and LF_NRRSP* control treated cells (**Fig. 1E)**. This phenotype is consistent with previous studies with RRSP and is possibly linked to cleavage of RAP1, which regulates cytoskeletal dynamics (32, 37, 40). Across all MEF cell lines, LF_NRRSP inhibited growth by at least 60% compared to PA only and LF_NRRSP* mutant controls (**Fig. 1F, Supplementary Fig. 1**). These data demonstrate that RRSP is able to target all isoforms of RAS to inhibit ERK phosphorylation and cell proliferation.

RRSP inhibits proliferation and pERK activation in colon cancer cell lines

In human cells, the dependency on KRAS for proliferation and survival can vary between cell lines, due to the impact of other oncogenic mutations in genes other than *RAS*. Singh et al. categorized several colon cancer cell lines for KRAS-dependency based on survival outcomes following *KRAS* RNAi silencing (36). Published data from our group has shown that the $KRAS^{Indep}$ cell line HCT-116 was highly susceptible to RRSP growth inhibition (27). To extend this finding, the effect of RRSP processing of RAS in $KRAS^{Dep}$ (SW620 and GP5d) and $KRAS^{Indep}$ (HCT-116, SW1463, HT-29) colon cancer cell lines was tested for relative susceptibility to RRSP (**Fig. 2A)**. However, due to the variable expression of the anthrax toxin receptor on the selected human cancer cells, we switched to a recently described, highly potent RRSP chimeric toxin wherein RRSP is tethered to the translocation B fragment of diphtheria toxin (RRSP-DT_B) (27). Similar to the anthrax toxin system, RRSP-DT_B binds to a human receptor (heparin binding epidermal growth factor-like growth factor (HB-EGF)), is endocytosed, and translocated into the cytosol across the vacuolar membrane. Expression of HB-EGF receptor was found to be similar between the selected colon cancer cell lines (**Supplementary Fig. 2A**).

To examine RRSP growth sensitivities between $KRAS^{Dep}$ versus $KRAS^{Indep}$ cell lines, colon cancer cells were treated with increasing concentration of RRSP-DT_B or with catalytically inactive RRSP-DT_B (RRSP*-DT_B) and growth inhibition was monitored. Contrary to prior studies with

siRNA knockdown of only KRAS, the $KRAS^{Indep}$ cell lines (HCT-116 and SW1463) showed the greatest sensitivity to loss of RAS due to RRSP in time lapse video microscopy. Cells treated with catalytically inactive RRSP* showed no difference, confirming the sensitivity was due to processing of RAS (**Fig. 2B and C, Supplementary Fig. 2B-E**). Unexpectedly, the $KRAS^{Dep}$ cell lines (SW620 and GP5d) showed some growth inhibition compared to cells treated with the control protein RRSP*-DT_B, but less than when compared to $KRAS^{Indep}$ cell lines (**Fig. 2E and 2G, Supplementary Fig. 2H-K**). Also contrary to the predicted outcome, HT-29 cells, expected to be resistant to RRSP due to a *BRAF-V600E* mutation, were highly susceptible (**Fig. 2D, Supplementary Fig. 2F and 2G**). Across all of the cell lines, at least 80% of total RAS was cleaved by RRSP (**Fig. 2H and 2I**). In addition, phosphorylation of ERK was significantly reduced compared to respective RRSP*-DT_B treated samples (**Fig. 2H and 2J**), except for cell line HT-29, in which pERK was unaffected due to the *BRAF V600E* mutation as expected.

These differences in growth and proliferation in response to RRSP also impacted long term survival. In RRSP highly susceptible cell lines HCT-116 and SW1463 cells, RRSP was highly cytotoxic compared to the mock treated control (**Fig. 3A**). By contrast, the highly sensitive cell line HT-29 showed no adverse cytotoxic effects in response to RRSP despite the observed growth inhibition. Data from time lapse imaging support this finding, where HT-29 cells treated with RRSP-DT_B formed massively rounded colonies that exhibited no obvious signs of cytotoxicity (**Supplementary Fig. 2L**). Cell lines less susceptible to RRSP, SW620 and GP5d, had similar effects, wherein viability remained unchanged in response to RRSP.

Altogether, these data suggest that while some cell lines are highly susceptible to RRSP resulting in cell death, some colon cancer cells remain viable despite loss of total RAS. To test if the changes are permanent, GP5d, SW620, and HT-29 cells were treated with phosphate buffered saline (PBS) or RRSP-DT_B for 48 hours and then reseeded at low cell densities for 14 days to examine colony formation. For each RRSP cell line, a decrease in colony formation ability compared to PBS control was observed (**Fig. 3B and 3C**), suggesting that RRSP can induce a

permanent non-proliferative state. SW620 cells had significant increase in activity of the senescence marker β-galactosidase, while β-galactosidase activity remained unchanged in HT-29 and GP5d cells (**Fig. 3D**). Altogether, these data demonstrate that RRSP is cytotoxic in some cell lines, while in less sensitive cell lines the cells remain viable but are unable to proliferate and, in some cases, enter into senescence.

RAS cleavage induces upregulation of CDK inhibitor, p27, in certain cell lines

We next took advantage of the unique cell line specific effects on cell growth and survival to better understand the underlying mechanisms regulating cell fate following RAS inhibition. Cell lysates from treated or untreated HCT-116 (highly sensitive) and SW620 (less sensitive) were incubated overnight with nitrocellulose membranes containing capture antibodies towards 43 different phosphorylated proteins. For RRSP treated HCT-116 cells, there was increased phosphorylation observed for cell stress proteins such as p38α, p90 ribosomal S6 kinase (RSK1/2/3), and Jun-activated kinase (JNK) (**Fig. 4A-C, Supplementary Fig.**). In addition, RRSP treatment increased phosphorylation of several Signal Transducer and Activator of Transcription (STAT) transcription factors. By contrast, the less responsive SW620 cells showed no observable changes in phosphorylation of similar cell stress enzymes and, notably, STAT protein phosphorylation was decreased (**Fig. 4A-C, Supplementary Fig. 3**). We observed a significant fold increase in With No K(lysine)-1 (WNK1) kinase at Thr-60. This kinase is best known for regulating ion transport across membranes (41). Little is known about mechanisms involved for WNK1 in cancer. Evidence has demonstrated that WNK1 Thr-60 phosphorylation is mediated by AKT in HEK293 cells. However, this modification has no effect on its kinase activity or its cellular localization (42). Because RRSP decreases AKT activation, it is unlikely that WNK1 Thr-60 phosphorylation is involved in the growth differences we observe between cell lines. We also observed a large fold-change difference observed between the two cell lines was phosphorylation

of CDK inhibitor p27 at Thr-198, wherein RRSP treatment increased p27 Thr-198 phosphorylation 12-fold in SW620 compared to HCT-116 (**Fig. 4C**). Previous studies have established this modification to be critical for stabilizing p27 expression by preventing ubiquitin-dependent degradation (43). In fact, aberrant RAS activity in cancer cells causes p27 post-translational downregulation through both ERK and AKT (10-12). These data support that inhibition of RAS by RRSP could lead to downstream rescue expression of p27 expression in cells, thereby slowing cell proliferation in cells. In fact, treatment with a sublethal dose of RRSP-DT_B increased p27 protein levels in HCT-116, SW620, and SW1463 cells, while GP5d and HT-29 levels remained unchanged (**Fig. 4D and 4E**). Concomitant with upregulation of p27, all cell lines, except HT-29, showed a significant decrease in RB phosphorylation at Ser-807/Ser-811 when treated with RRSP-DT_B (**Fig. 4D and 4F**). Unfortunately, total RB was undetectable using commercially available antibodies, except in HT-29. To be confident that RB hypo-phosphorylation was not due to low RB expression, we transiently expressed green-fluorescent protein (GFP)-tagged RB in HCT-116 cells (**Supplementary Fig. 4B**). In GFP-RB expressing cells treated with RRSP-DT_B, hypo-phosphorylation of RB protein compared to PBS and RRSP*-DT_B controls was observed (**Supplementary Fig. 4C**). Protein levels of GFP-RB decreased in RRSP-DT_B, consistent with a role of p27 in regulating RB expression (44).

Unexpectedly, hypo-phosphorylation of RB was observed also in GP5d cells despite showing no change in the expression or phosphorylation of p27. The CDK inhibitor p21 also plays a critical role in RB regulation. However, in GP5d cells, RRSP showed no change in p21 protein levels, suggesting that RB hypo-phosphorylation in RRSP treated cells is both p21 and p27 independent (**Supplementary Fig. 4D**). This finding suggest RRSP may inhibit cancer cell growth through other as yet unknown signaling networks that can negatively impact cell growth.

RRSP induces G1 phase cycle arrest in KRAS mutant cell lines

Elevated p27 protein expression in combination with hypo-phosphorylation of RB suggested that RRSP treatment induced a cell cycle arrest in colon cancer cells. Under normal conditions, p27 regulates G1 checkpoint during the cell cycle by preventing entry into S phase through inhibition of CDKs 2/4/6 (8, 9). To test if RRSP-DT_B treatment induces cell cycle arrest, cell lines were treated for 24 hours and the percentage of cells in G1, S, or G2/M phase was monitored by flow cytometry. Among RRSP-DT_B treated cells, all KRAS mutant cell lines that showed reduced RB phosphorylation had significant population of cells locked in the G1 state compared to PBS and RRSP*-DT_B treated samples (**Fig. 5, Supplementary Fig. 6**). The most dramatic increase in G1 arrest was seen in SW620 cells, where nearly 100% of cells remained in the G0/G1 phase following RRSP-DT_B treatment (**Fig. 5D**). This G1 cell arrest was dependent of the RAS processing activity of RRSP as the catalytically inactive mutant RRSP-DT_B did not induce the cell cycle arrest (**Fig. 5D**). However, despite HT-29 cells being unable to proliferate following RRSP treatment, these cells remained unchanged in cell cycle response, suggesting RRSP growth inhibition in some instances does not occur through cell cycle inhibition. Coupled with the observation that these cells are enlarged (**Supplementary Fig. 2L**), this observation suggests that HT-29 cells undergo chromosome replication but fail to undergo cell division. Together, these data illustrate that RRSP cleavage of RAS can induce growth inhibition through several different mechanisms, some of which are still only partially understood.

Discussion

It has been over 30 years since the discovery of the importance of RAS for driving tumorigenesis in cancer. Lung, pancreatic, and colon cancers remain being the most lethal cancers in the United States with high mutation rates in RAS, the most commonly mutated isoform of KRAS. Despite the significant amount of research being conducted on RAS, it still remains a challenging target in the field. Small molecules directed to specific RAS mutants, specially KRAS

G12C, have shown promising results in clinical trials (45), but will only benefit a small subset of patients. Our lab has discovered RRSP as a potent, site specific inhibitor of RAS capable of inhibiting all RAS isoforms simultaneously along with downstream activation. RRSP antitumorigenic effects are well demonstrated *in vivo* with xenograft models for both breast and colon cancers, wherein tumor growth was stunted and, in some cases, showed regression (27). Evidence for RRSP as a therapeutic inhibitor of RAS is sufficient, however its applicability and effectiveness across different cancer cell lines harboring varying mutations in RAS still remains an outstanding question. In this study, we examined the signaling consequences of cleavage of all RAS in several colon cancer cell lines and its downstream implications on cell proliferation and survival.

First, we examined whether RRSP was a suitable inhibitor across RAS variants. Using the RAS-less MEF model, we demonstrated that all three major RAS isoforms and frequently observed KRAS mutants (G12V, G12D, G13D, G12C, and Q61R) were equivalent substrates for RRSP. In each cell line tested, we observed at least a 75% reduction of total RAS after 24 hours of RRSP treatment. Loss of RAS resulted in reduced ERK activation, which as expected, negatively affected proliferation in each cell line. More importantly, we observed no significant differences in RAS cleavage between wildtype isoforms and KRAS mutants, highlighting that RRSP-directed RAS inhibition could be a useful tool to study the impact of RAS inhibition independently of mutation or isoform differences.

We next examined RRSP effectiveness in cancer cell lines with varying dependencies on KRAS. In both $KRAS^{Indep}$ and $KRAS^{Dep}$ cell lines, we observed modest to severe growth inhibition from all five cell lines examined. To our surprise, the two $KRAS^{Indep}$ cell lines (HCT-116 and SW1463) were the most sensitive to RRSP treatment. Conversely, $KRAS^{Dep}$ cell lines (GP5d and SW620) were moderately affected by RRSP treatment. These data suggest that the varying growth responses seen between cells lines are likely due to the unique ability to target all RAS in cells. As RRSP is able to eliminate activity of all RAS isoforms in cells, not just KRAS, it is possible

that growth can be inhibited in both $KRAS^{Dep}$ and $KRAS^{Indep}$ cell lines. Most surprisingly was the response we observed in HT-29 cells, which harbor a BRAF V600E mutation, which showed growth sensitivities comparable to HCT-116 and SW620 cell lines.

We further examined if the observed RRSP-dependent growth inhibition also impacted cell survival. Two of the cell lines with the greatest RRSP growth sensitivity, HCT-116 and SW1463, had lower metabolic activity compared to controls indicting cytotoxicity in response to RRSP. Interestingly, GP5d, SW620, and HT-29 all remained viable despite lacking the ability to proliferate. We next asked if RRSP growth inhibition in these cells was transient or permanent. Surprisingly, all three noncytotoxic cell lines showed significant inability to form colonies following RRSP treatment, mimicking a senescent-like phenotype. From the three cell lines tested, SW620 cells had elevated β-galactosidase activity indicting RRSP could also activate senescent-like mechanisms.

We then pursued the signaling mechanisms responsible for the different outcomes observed between cell lines, in particular cytotoxic versus noncytotoxic RRSP treated cell lines. To this end, we examined the phosphorylation status of 43 different signaling kinases between HCT-116 (highly sensitive) and SW620 (less sensitive) cells treated with a sublethal dose of RRSP. The most significant hit from the screen was differential phosphorylation of critical CDK inhibitor p27. Indeed, all of the cell lines, except HT-29, showed significantly increased p27 protein levels as a result of RAS cleavage. We also observed hypo-phosphorylation of RB protein in RRSP-treated cell lines and that RRSP treated cells are locked in the G1 phase. We demonstrate that this occurs through the p27 tumor suppressor, which is post-translationally suppressed in RAS-driven cancers. To our surprise, cytotoxic RRSP cell lines, HCT-116 and SW1463, also showed signs of p27 dependent growth arrest. These data suggest that RAS cleavage in certain colon cancer cells induces p27 upregulation, leading to a cell cycle arrest state that can induce cell death at prolonged timepoints. This effect has been well illustrated in several cancer cell lines where transient overexpression of p27 induces cell cycle arrest and later apoptosis (46, 47).

RRSP-induced cell cycle arrest has recently been observed also in HeLa cells. RRSP is conserved a domain found on a toxin from *Photorhabdus asymbiotica.* RRSP from *P. asymbiotica* has shown to cleave RAS (32) and recently reported to induce G1 cell cycle arrest (48). The proposed mechanism involved direct binding of RRSP to cyclin dependent kinase 1 inhibition (CDK1) when the protein is transiently overexpressed. Thus, the multi-domain RRSP may possess independent mechanisms for growth inhibition.

The most unique phenotype from our data was shown in HT-29 cells in which RRSP severely affected proliferation, but not reduce viability or cell cycle checkpoints. Thus, these cells still undergo DNA replication, but may continue to expand without undergoing cell division. Due to the activating mutation in *BRAF*, we propose that RRSP-dependent growth inhibition in this case may be RAS-independent. Because RRSP also targets RAP1, a critical regulator of cytokinesis, it is possible that cleavage of RAP1 plays a role in growth inhibition making cells unable to divide. Previous studies have suggested that RAP1 inactivation could lead to growth abnormalities independently of the cell cycle (49). The role RAP1 plays in proliferation through regulating mitosis related activity remains to be investigated but could provide an alternative target for cancer targeting strategies.

Here we provide evidence of the mechanism by which RRSP affects growth inhibition in colon cancer cells. Cells with proliferative defects through RAS have restoration of p27 protein expression that leads to cell cycle arrest. These data further highlight the unique antitumor properties of RRSP that can be applicable across different KRAS mutants, with broad impact as it may target distinct pathways in different tumors. Notably, because low p27 expression levels have been correlated with poor survival in patients with different types of cancer including colon, the ability of RRSP to restore p27 expression as a consequence of RAS inhibition might have important implications for the treatment of tumors with aberrant RAS signaling.

Materials and Methods

Cell Lines

'RAS-less' mouse embryonic fibroblast (MEF) cells were provided by the NCI RAS Initiative at Frederick National Laboratory for Cancer Research (FNLCR). HCT-116 cells were purchased from the American Type Culture Collection. SW1463, GP5d, and SW620 were provided by the NCI. HT-29 cells were provided from the Marcus Peter lab at Northwestern University. Each cell line was validated by the Northwestern University Sequencing Core by Short Tandem Repeat profiling.

All cells were cultured at 37°C and 5% CO_2 atmosphere. HCT-116, SW1463, GP5d, SW620 cells were cultured in Dulbecco's Modified Eagle Medium (DMEM)-F12 with Glutamax (Gibco) containing 10% fetal bovine serum (FBS; Gemini Bio) and 1% penicillin/streptomycin (P/S; Invitrogen). HT-29 cells were cultured in RPMI-1640 (Gibco) containing 10% FBS and 1% P/S. All MEF cells, except for HRAS RAS-less MEFs, were cultured in DMEM (Gibco) with 10% FBS,1% P/S, and 4 μg/ml of blasticidin (ThermoFisher Scientific). HRAS MEFs was cultured in 2.5 μg/ml of puromycin (ThermoFisher Scientific).

Antibodies

Anti-RAS monoclonal antibody recognizing G-domain of all major RAS isoforms was purified from a hybridoma cell line provided by FNLCR and used at 1:2000 dilution as previously described (27). Other commercially available primary antibodies used were: anti–Phospho-p44/42 MAPK (phosphorylated ERK1/2, Thr202/Tyr204, Cell Signaling Technology #4377), anti-p44/42 MAPK (ERK1/2, Cell Signaling Technology #4696), anti-HB-EGF (R&D Systems, #AF-259-NA;), anti-$p27^{Kip1}$ XP (Cell Signaling Technology #3686), Phospho-RB (Ser807/Ser811, Cell Signaling Technology #8516), anti-$p16^{INKa}$ (R&D Systems #AF5779-SP), anti-$p21^{WAF/Cip1}$ (Cell Signaling Technology #2947T), anti-α-Tubulin (Cell Signaling Technology #2144), and anti-vinculin (Cell Signaling Technology #13901). Fluorescently-labeled secondary antibodies obtained from LI-

COR Biosciences and used at 1:10,000 dilution were: IRDye 680RD goat anti-mouse (926-68070), IRDye 800CW goat anti-rabbit (925-322211), and IRDye 800CW donkey anti-goat (925-32214). Western blot images were acquired using an Odyssey Infrared Imaging System (LI-COR Biosciences) and quantified by densitometry using NIH ImageJ software.

pRB-GFP Transfection

Plasmid RB-GFP FL for expression of GFP-tagged RB was obtained from Addgene (Catalog #16004). For ectopic gene expression, cell lines were transfected using FuGene HD (Promega) according to the manufacturer's protocols. GFP fluorescence was analyzed using EVOS XL Core imaging system.

Western Blotting

Cells were washed in PBS and then resuspended in lysis buffer [150 mM NaCl, 20 mM Tris (pH 7.5), 1% Triton X-100, and Pierce Protease phosphatase inhibitor (Sigma-Aldrich)]. Lysates were incubated for 15 minutes on ice and centrifuged at 20,000 x *g* at 4°C for 15 minutes. The concentration of protein in the collected supernatant fluid was determined using the bicinchoninic acid (BCA) assay (ThermoFisher Scientific, no. 23227). Samples were boiled at 95°C in Laemmli SDS loading buffer for 10 minutes and protein was separated on either 15 or 18% SDS–polyacrylamide gels. Proteins were transferred to nitrocellulose membranes and blocked in Tris-buffered saline (TBS) [10 mM Tris (pH 7.4) and 150 mM NaCl] with 5% (w/v) milk for 1 hour. Membranes were washed with TBS and then incubated in indicated primary antibodies in TBS with 5% (w/v) Fraction V bovine serum album (Fisher BioReagents #194850) overnight at 4°C. Total percentage RAS was calculated using the following equation: % Total RAS = uncleaved RAS band / (RAS uncleaved band / RAS cleaved band) X 100.

Purification and Intoxication of LF_NRRSP in MEFs

Recombinant LF_NRRSP and LF_NRRSP* were expressed in *Escherichia coli* BL21(DE3) and purified over a HisTrap FF nickel affinity column followed by Superdex 75 size exclusion chromatography using the ÄKTA protein purifier purification system (GE Healthcare), as previously described (37). For intoxication, MEFs were seeded in 6-well plates at 3 x 10^5 cells per well for 1 hour, after which medium was replaced with fresh medium containing with 7 nM Protective antigen (PA) alone (List Labs, #171E) or in the presence of 3 nM LF_NRRSP/ LF_NRRSP^{H4030A} and incubated at indicated timepoints at 37°C in the presence of 5% CO_2.

Purification and Intoxication of RRSP-DT_B in Colon Cancer Cell Lines

Recombinant RRSP-DT_B and RRSP*-DT_B were expressed in *E. coli* BL21(DE3) and purified over a HisTrap FF nickel affinity column as previously described (27). Eluted fractions were loaded onto a gravity column containing Strep-Tactin Superflow high capacity resin, followed by SUMO-tag removal and size exclusion purification over a Superdex 75 column using ÄKTA protein purifier purification system as previously described (27). For intoxication, colon cancer cell lines were seeded in 6-well plates (~70% confluency) overnight, after which medium was replaced with fresh medium containing either RRSP-DT_B or RRSP*-DT_B and incubated at indicated timepoints at 37°C in the presence of 5% CO_2.

Time-Lapse Video Microscopy

For RAS-less MEFs (6 x 10^3 cells per well) were cultured in 96-well clear bottom white plates in corresponding complete growth medium and treated after 4 hours with RRSP-DT_B or RRSP*-DT_B. Colorectal cancer cell lines were plated at ~80% confluency and cultured in 96-well clear bottom white plates. Complete growth medium with RRSP-DT_B or RRSP*-DT_B was added after overnight cell attachment. All cells were cultured were in Nikon Biostation CT and images were taken at indicated timepoints. Cell confluency was quantified using Nikon Elements software. IC_{50} concentrations were calculated using log(inhibitor) vs. response variable slope (four parameters) function in Graphpad Prism 8.

Cell Viability and Cell Survival Assays

Colon cancer cell lines were seeded in 96-well clear bottom white plates at ~80% confluency. Complete growth medium with RRSP-DT_B or RRSP*-DT_B was added after overnight cell attachment. After 72 hours, CellTiter-Glo (Promega) reagent was added to each well and luminescence was detected using Tecan Safire2 plate reader. For crystal violet assays, cells were treated as described above and were incubated for 48 hours. Following incubation cells were harvested and reseeded at low seeding densities in 6-well plates. Colony formation was monitored over 14 days, during which media was replaced every three days. On day 14 colonies were fixed in crystal violet fixing/staining solution (0.05% (g/vol) crystal violet, 1% formaldehyde, 1% (v/v) methanol in PBS. Open source ColonyArea ImageJ plug-in was used for quantitative analysis of the area % covered by the stained colonies (38). Due to high background from crystal violet staining in SW620 cells, stained wells were dissolved in 10% acetic acid and destained on rocker for 30 minutes. Absorbance was measured at 590 nm using Tecan Safire2 plate reader.

Proteome Human Phospho-Kinase Array

Colon cancer cell lines were treated as described and washed in 1X PBS. Cells were solubilized using lysis buffer provided by the vendor (R&D Systems) and rocked for 30 minutes at 4°C. Suspension was spun for 5 minutes at 14,000 x *g* and supernatant was collected. Concentration of protein in the collected supernatant fluid determined using the BCA assay (ThermoFisher Scientific, no. 23227). 200 µg of sample lysate was applied to nitrocellulose membranes kinase arrays and incubated overnight at 4°C. Provided detection antibodies were incubated with specified concentrations as suggested by the supplier. Membrane arrays were acquired using Odyssey Infrared Imaging System (LI-COR Biosciences) and quantified by densitometry using NIH ImageJ software.

Cell cycle flow cytometry

Colon cancer cell lines were treated as described above. After 24 hours of treatment, cells were collected from medium, washed with 1X PBS, and released from well with Trypsin-EDTA (0.25%), phenol red (Invitrogen). Harvested cells were centrifuged at 700 x *g* for 5 minutes. Cells were again washed in PBS and spun down at 700 x *g* for 5 minutes. PBS was removed and cells were resuspended in 600 µL of ice-cold PBS. Cell were permeabilized with addition of 1.4 mL of ice-cold ethanol slowly and incubated overnight at -20°C. Following two washes with PBS (centrifuged at 700 x *g* for 5 minutes), cells were stained in 200 µL PI staining solution (1% Triton X-100, 50 µg propidium iodide (BioLegend), 100 µg RNase) for 30 minutes. Samples were analyzed on BD LSR Fortessa 1 Analyzer. At least 10,000 events were collected for each sample. Single cell populations were viewed and gated on cyanine-3 area (Cy3-A) versus cyanine-3 width (Cy3-W) channels, to eliminate doublet events. ModFit LT Software (Version 5) was used for cell cycle analysis.

Disclosure of Potential Conflicts of Interest

K.J.F.S. has been granted a patent (US 10,829,752 B2) on use of RRSP to treat cancer. K.J.F.S. is a consultant for Buoy Health on topics unrelated to this manuscript. K.J.F.S. has a significant financial interest in Situ Biosciences, LLC, a contract research organization that pursues research unrelated to cancer. C.K.S. is an intern as a scientific and financial advisor for Aspire Capital Partners, LLC, which invests in oncotherapies.

Authors' Contributions

C.K.S. designed and conducted all experiments and wrote the manuscript. M.B. conducted preliminary experiments with the Ras-less MEF cells. V.V. contributed reagents, assisted with

experimental design, and edited the manuscript. K.J.F.S. oversaw all aspects of design, conduct, and analysis of the experiments and edited the manuscript.

Acknowledgments

We thank the Frederick National Laboratory for Cancer Research (FNLCR) for providing the RAS-less MEF cells, KRAS mutant cell lines, and hybridoma cells for the pan-RAS antibody directed against the G-domain. Marcus Peter lab is thanked for providing HT-29 cell line. Matthew Kieffer and all members of the Satchell laboratory are thanked for valuable intellectual input and technical support. This work was funded by grants from the Chicago Biomedical Consortium, H Foundation, Northwestern Medicine Catalyst Fund, and National Institute of Health R01 AI092825 (to K.J.F.S). C.K.S. was supported by a fellowship from the National Cancer Institute (T32 CA09560). High content imaging was performed on the Nikon Biostation CT system purchased with the support of NIH grant S10 OD021704. Flow cytometry core services were provided by the Northwestern University RHLCCC Flow Cytometry Facility supported by NIH grant P30 CA060553.

Footnotes:

Note: Supplementary data for this article (Suppl. Fig. 1-6)

References

1. Hobbs GA, Der CJ, Rossman KL. RAS isoforms and mutations in cancer at a glance. J Cell Sci. 2016;129(7):1287-92.

2. Bos JL, Rehmann H, Wittinghofer A. GEFs and GAPs: critical elements in the control of small G proteins. Cell. 2007;129(5):865-77.

3. Vigil D, Cherfils J, Rossman KL, Der CJ. Ras superfamily GEFs and GAPs: validated and tractable targets for cancer therapy? Nat Rev Cancer. 2010;10(12):842-57.

4. Cox AD, Fesik SW, Kimmelman AC, Luo J, Der CJ. Drugging the undruggable RAS: Mission possible? Nat Rev Drug Discov. 2014;13(11):828-51.

5. Downward J. Targeting RAS signalling pathways in cancer therapy. Nat Rev Cancer. 2003;3(1):11-22.

6. Drosten M, Dhawahir A, Sum EY, Urosevic J, Lechuga CG, Esteban LM, et al. Genetic analysis of Ras signalling pathways in cell proliferation, migration and survival. EMBO J. 2010;29(6):1091-104.

7. Pruitt K, Pestell RG, Der CJ. Ras inactivation of the retinoblastoma pathway by distinct mechanisms in NIH 3T3 fibroblast and RIE-1 epithelial cells. J Biol Chem. 2000;275(52):40916-24.

8. Hengst L, Reed SI. Inhibitors of the Cip/Kip family. Curr Top Microbiol Immunol. 1998;227:25-41.

9. Sherr CJ, Roberts JM. CDK inhibitors: positive and negative regulators of G1-phase progression. Genes Dev. 1999;13(12):1501-12.

10. Kerkhoff E, Rapp UR. Induction of cell proliferation in quiescent NIH 3T3 cells by oncogenic c-Raf-1. Mol Cell Biol. 1997;17(5):2576-86.

11. Greulich H, Erikson RL. An analysis of Mek1 signaling in cell proliferation and transformation. J Biol Chem. 1998;273(21):13280-8.

12. Rivard N, Boucher MJ, Asselin C, L'Allemain G. MAP kinase cascade is required for p27 downregulation and S phase entry in fibroblasts and epithelial cells. Am J Physiol. 1999;277(4):C652-64.

13. Hayashi H, Ogawa N, Ishiwa N, Yazawa T, Inayama Y, Ito T, et al. High cyclin E and low p27/Kip1 expressions are potentially poor prognostic factors in lung adenocarcinoma patients. Lung Cancer. 2001;34(1):59-65.

14. Loda M, Cukor B, Tam SW, Lavin P, Fiorentino M, Draetta GF, et al. Increased proteasome-dependent degradation of the cyclin-dependent kinase inhibitor p27 in aggressive colorectal carcinomas. Nat Med. 1997;3(2):231-4.

15. Masciullo V, Ferrandina G, Pucci B, Fanfani F, Lovergine S, Palazzo J, et al. p27Kip1 expression is associated with clinical outcome in advanced epithelial ovarian cancer: multivariate analysis. Clin Cancer Res. 2000;6(12):4816-22.

16. Mineta H, Miura K, Suzuki I, Takebayashi S, Amano H, Araki K, et al. Low p27 expression correlates with poor prognosis for patients with oral tongue squamous cell carcinoma. Cancer. 1999;85(5):1011-7.

17. Pohl G, Rudas M, Dietze O, Lax S, Markis E, Pirker R, et al. High p27Kip1 expression predicts superior relapse-free and overall survival for premenopausal women with early-stage breast cancer receiving adjuvant treatment with tamoxifen plus goserelin. J Clin Oncol. 2003;21(19):3594-600.

18. Tsihlias J, Kapusta LR, DeBoer G, Morava-Protzner I, Zbieranowski I, Bhattacharya N, et al. Loss of cyclin-dependent kinase inhibitor p27Kip1 is a novel prognostic factor in localized human prostate adenocarcinoma. Cancer Res. 1998;58(3):542-8.

19. Chin L, Tam A, Pomerantz J, Wong M, Holash J, Bardeesy N, et al. Essential role for oncogenic Ras in tumour maintenance. Nature. 1999;400(6743):468-72.

20. Collins MA, Brisset JC, Zhang Y, Bednar F, Pierre J, Heist KA, et al. Metastatic pancreatic cancer is dependent on oncogenic Kras in mice. PLoS One. 2012;7(12):e49707.

21. Fisher GH, Wellen SL, Klimstra D, Lenczowski JM, Tichelaar JW, Lizak MJ, et al. Induction and apoptotic regression of lung adenocarcinomas by regulation of a K-Ras transgene in the presence and absence of tumor suppressor genes. Genes Dev. 2001;15(24):3249-62.

22. Kwong LN, Costello JC, Liu H, Jiang S, Helms TL, Langsdorf AE, et al. Oncogenic NRAS signaling differentially regulates survival and proliferation in melanoma. Nat Med. 2012;18(10):1503-10.

23. Ying H, Kimmelman AC, Lyssiotis CA, Hua S, Chu GC, Fletcher-Sananikone E, et al. Oncogenic Kras maintains pancreatic tumors through regulation of anabolic glucose metabolism. Cell. 2012;149(3):656-70.

24. Janes MR, Zhang J, Li LS, Hansen R, Peters U, Guo X, et al. Targeting KRAS Mutant Cancers with a Covalent G12C-Specific Inhibitor. Cell. 2018;172(3):578-89 e17.

25. Ostrem JM, Peters U, Sos ML, Wells JA, Shokat KM. K-Ras(G12C) inhibitors allosterically control GTP affinity and effector interactions. Nature. 2013;503(7477):548-51.

26. Patricelli MP, Janes MR, Li LS, Hansen R, Peters U, Kessler LV, et al. Selective Inhibition of Oncogenic KRAS Output with Small Molecules Targeting the Inactive State. Cancer Discov. 2016;6(3):316-29.

27. Vidimar V, Beilhartz GL, Park M, Biancucci M, Kieffer MB, Gius DR, et al. An engineered chimeric toxin that cleaves activated mutant and wild-type RAS inhibits tumor growth. Proc Natl Acad Sci U S A. 2020;117(29):16938-48.

28. Yingwei Chen EAT, Biao Ruan, Eun Jung Choi, Richard Simmerman, Yihong Chen, Yanan He, Ruixue Wang, Raquel Godoy-Ruiz, Harlan King, Gregory Custer, D. Travis Gallagher, David A. Rozak, Melani Solomon, Silvia Muro, David J. Weber, John Orban, Thomas R. Fuerst, Philip N. Bryan. Engineering protein-specific proteases: targeting active RAS. bioRxiv. 2020.

29. Roth S, Macartney TJ, Konopacka A, Chan KH, Zhou H, Queisser MA, et al. Targeting Endogenous K-RAS for Degradation through the Affinity-Directed Protein Missile System. Cell Chem Biol. 2020;27(9):1151-63 e6.

30. Gavin HE, Beubier NT, Satchell KJ. The Effector Domain Region of the Vibrio vulnificus MARTX Toxin Confers Biphasic Epithelial Barrier Disruption and Is Essential for Systemic Spread from the Intestine. PLoS Pathog. 2017;13(1):e1006119.

31. Gavin HE, Satchell KJF. RRSP and RID Effector Domains Dominate the Virulence Impact of Vibrio vulnificus MARTX Toxin. J Infect Dis. 2019;219(6):889-97.

32. Antic I, Biancucci M, Zhu Y, Gius DR, Satchell KJ. Site-specific processing of Ras and Rap1 Switch I by a MARTX toxin effector domain. Nat Commun. 2015;6:7396.

33. Biancucci M, Minasov G, Banerjee A, Herrera A, Woida PJ, Kieffer MB, et al. The bacterial Ras/Rap1 site-specific endopeptidase RRSP cleaves Ras through an atypical mechanism to disrupt Ras-ERK signaling. Sci Signal. 2018;11(550).

34. Biancucci M, Rabideau AE, Lu Z, Loftis AR, Pentelute BL, Satchell KJF. Substrate Recognition of MARTX Ras/Rap1-Specific Endopeptidase. Biochemistry. 2017;56(21):2747-57.

35. Chabner BA. NCI-60 Cell Line Screening: A Radical Departure in its Time. J Natl Cancer Inst. 2016;108(5).

36. Singh A, Sweeney MF, Yu M, Burger A, Greninger P, Benes C, et al. TAK1 inhibition promotes apoptosis in KRAS-dependent colon cancers. Cell. 2012;148(4):639-50.

37. Antic I, Biancucci M, Satchell KJ. Cytotoxicity of the Vibrio vulnificus MARTX toxin effector DUF5 is linked to the C2A subdomain. Proteins. 2014;82(10):2643-56.

38. Guzman C, Bagga M, Kaur A, Westermarck J, Abankwa D. ColonyArea: an ImageJ plugin to automatically quantify colony formation in clonogenic assays. PLoS One. 2014;9(3):e92444.

39. Loftis AR, Santos MS, Truex NL, Biancucci M, Satchell KJF, Pentelute BL. Anthrax Protective Antigen Retargeted with Single-Chain Variable Fragments Delivers Enzymes to Pancreatic Cancer Cells. Chembiochem. 2020;21(19):2772-6.

40. Bos JL. Linking Rap to cell adhesion. Curr Opin Cell Biol. 2005;17(2):123-8.

41. Gallolu Kankanamalage S, Karra AS, Cobb MH. WNK pathways in cancer signaling networks. Cell Commun Signal. 2018;16(1):72.

42. Vitari AC, Deak M, Collins BJ, Morrice N, Prescott AR, Phelan A, et al. WNK1, the kinase mutated in an inherited high-blood-pressure syndrome, is a novel PKB (protein kinase B)/Akt substrate. Biochem J. 2004;378(Pt 1):257-68.

43. Schiappacassi M, Lovisa S, Lovat F, Fabris L, Colombatti A, Belletti B, et al. Role of T198 modification in the regulation of p27(Kip1) protein stability and function. PLoS One. 2011;6(3):e17673.

44. Broude EV, Swift ME, Vivo C, Chang BD, Davis BM, Kalurupalle S, et al. p21(Waf1/Cip1/Sdi1) mediates retinoblastoma protein degradation. Oncogene. 2007;26(48):6954-8.

45. Goebel L, Muller MP, Goody RS, Rauh D. KRasG12C inhibitors in clinical trials: a short historical perspective. Rsc Med Chem. 2020;11(7):760-70.

46. Schreiber M, Muller WJ, Singh G, Graham FL. Comparison of the effectiveness of adenovirus vectors expressing cyclin kinase inhibitors p16INK4A, p18INK4C, p19INK4D, p21(WAF1/CIP1) and p27KIP1 in inducing cell cycle arrest, apoptosis and inhibition of tumorigenicity. Oncogene. 1999;18(9):1663-76.

47. Wang X, Gorospe M, Huang Y, Holbrook NJ. p27Kip1 overexpression causes apoptotic death of mammalian cells. Oncogene. 1997;15(24):2991-7.

48. Wang X, Shen J, Jiang F, Jin Q. The Photorhabdus Virulence Cassettes RRSP-Like Effector Interacts With Cyclin-Dependent Kinase 1 and Causes Mitotic Defects in Mammalian Cells. Front Microbiol. 2020;11:366.

49. Dao VT, Dupuy AG, Gavet O, Caron E, de Gunzburg J. Dynamic changes in Rap1 activity are required for cell retraction and spreading during mitosis. J Cell Sci. 2009;122(Pt 16):2996-3004.

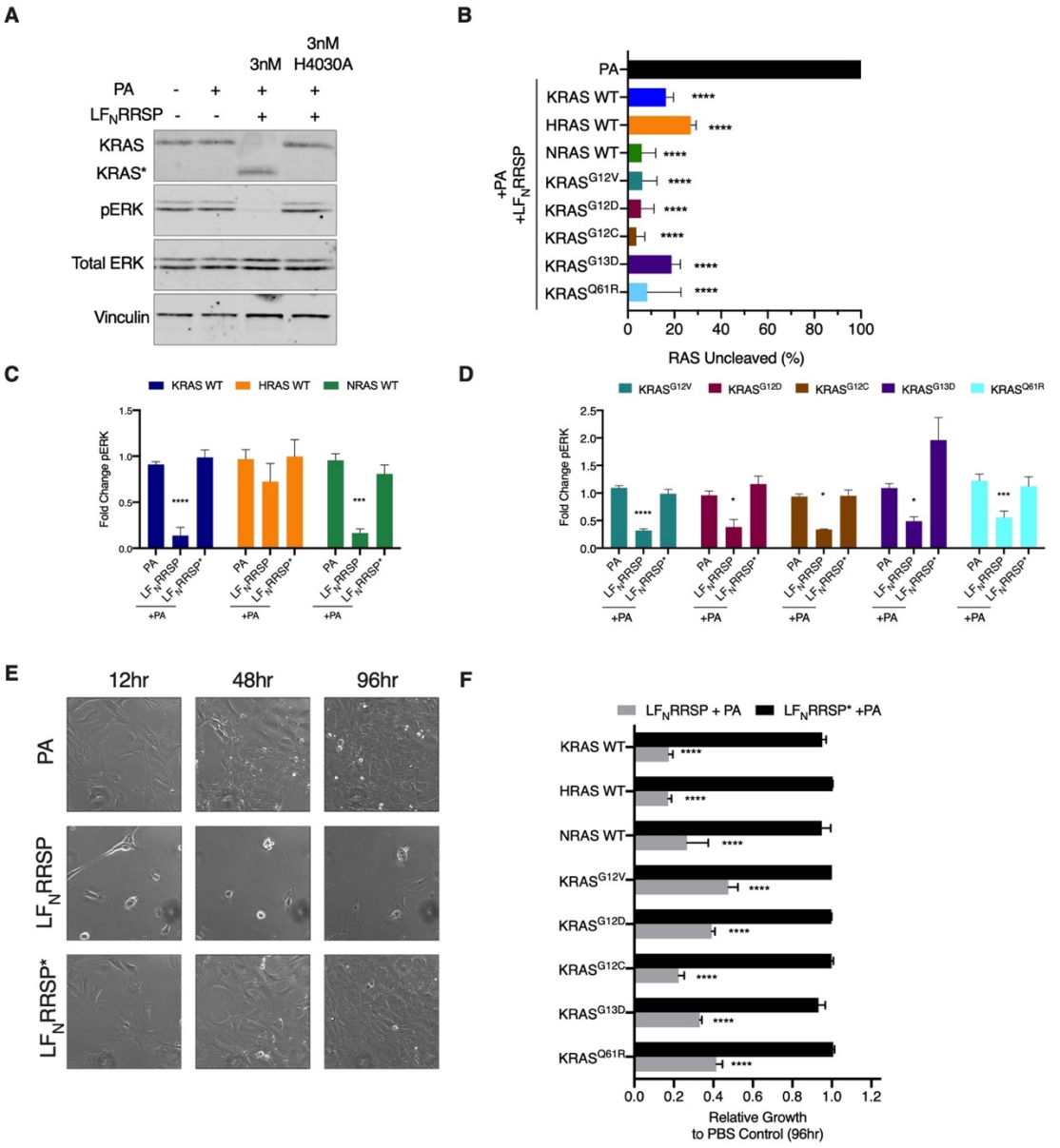

Figure 1. LF_NRRSP cleaves and inhibits all RAS isoforms and KRAS oncogenic mutants in RAS-less MEFs. (**A**) Representative western blot analysis of LF_NRRSP cleavage of RAS and inhibition of ERK in KRAS WT RAS-less MEFs after 24 hr. Vinculin was used as a gel loading control. (**B**) Densitometric analysis of total percent RAS following LF_NRRSP treatment after 24 hr in RAS-less MEF cell lines; *n* = 3. (**C and D**) Densitometric analysis of fold change in pERK compared to PBS control after 24 hr for RAS-less MEF cell lines described; *n* = 3. (**E**) Brightfield images of KRAS WT RAS-less MEFs treated with either PA alone or in combination with LF_NRRSP or LF_NRRSP* at indicated timepoints. (**F**) Relative growth inhibition in RAS-less MEFs compared to PA control at 96 hours following treatment with either LF_NRRSP or LF_NRRSP*. Results are expressed as mean ± SEM of three independent experiments (*P<0.05, **P<0.01, ****P<0.0001 versus PA control as determined through one-way ANOVA followed by Dunnett's multiple comparison test).

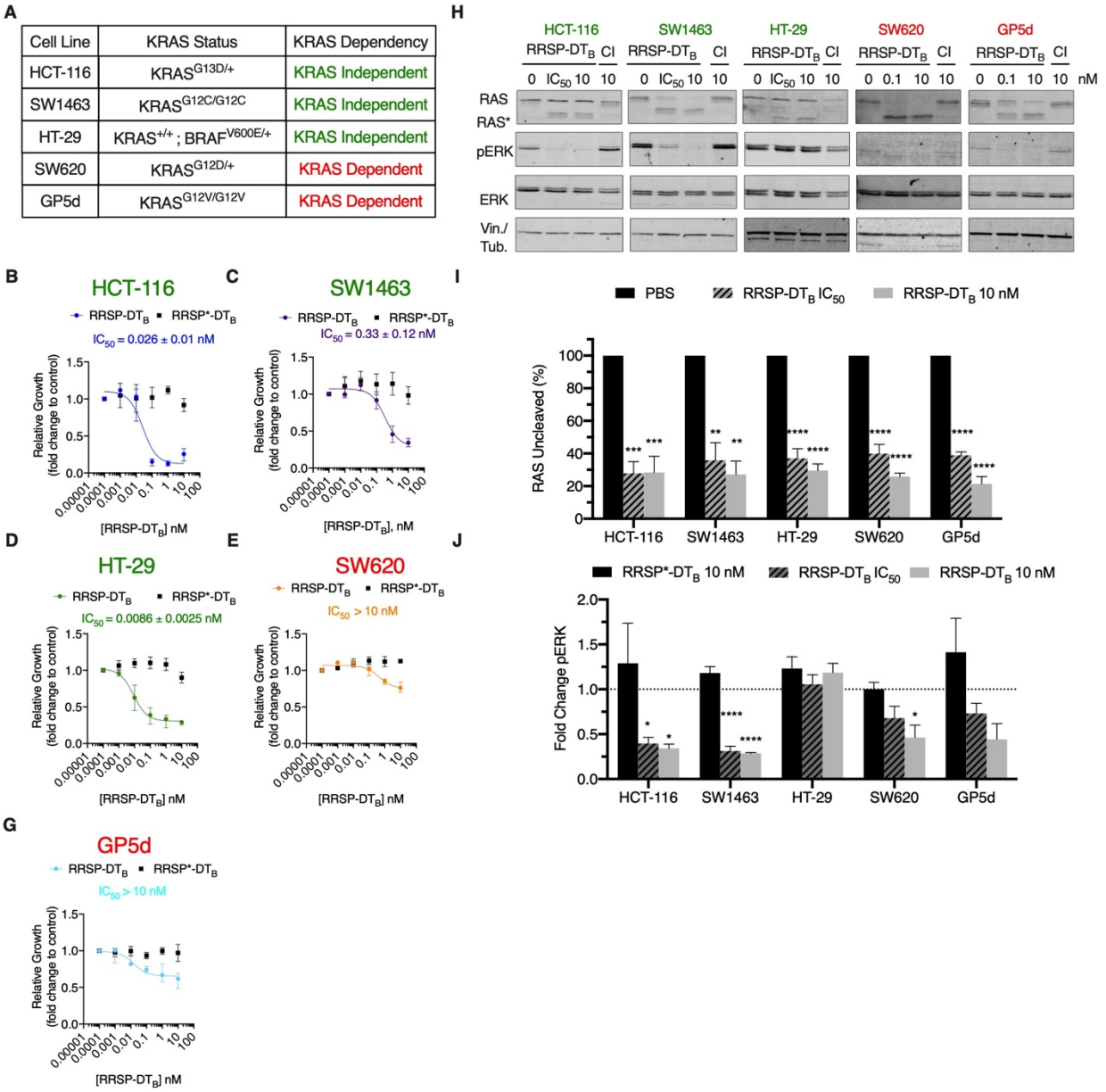

Figure 2. RRSP-DT$_B$ growth inhibition in KRAS-dependent and independent colon cancer cell lines as defined by (36). (**A**) Cell line panel of KRAS dependent and independent colon cancer cells. (**B-G**) Fitted dose response curve of RRSP-DT$_B$ in colon cancer cell lines after 24 hr. Results are displayed as mean ± SEM, *n* = 4. (**H**) Representative western blot analysis of RAS cleavage and ERK inhibition in colon cancer cell lines treated with either RRSP-DT$_B$ or catalytically inactive mutant (labeled by CI) after 24 hr. All concentrations are expressed in nanomolar. In all cell lines, vinculin was used as gel loading control except SW620 cells in which αTubulin was used. (**I** and **J**) Densitometric analysis of fold change in percent total RAS and pERK compared to PBS control after 24 hours in colon cancer cell lines; *n* = 3. Results are expressed as means ± SD of three independent experiments (*P<0.05, **P<0.01, ****P<0.0001 versus PBS control as determined through one-way ANOVA followed by Dunnett's multiple comparison test).

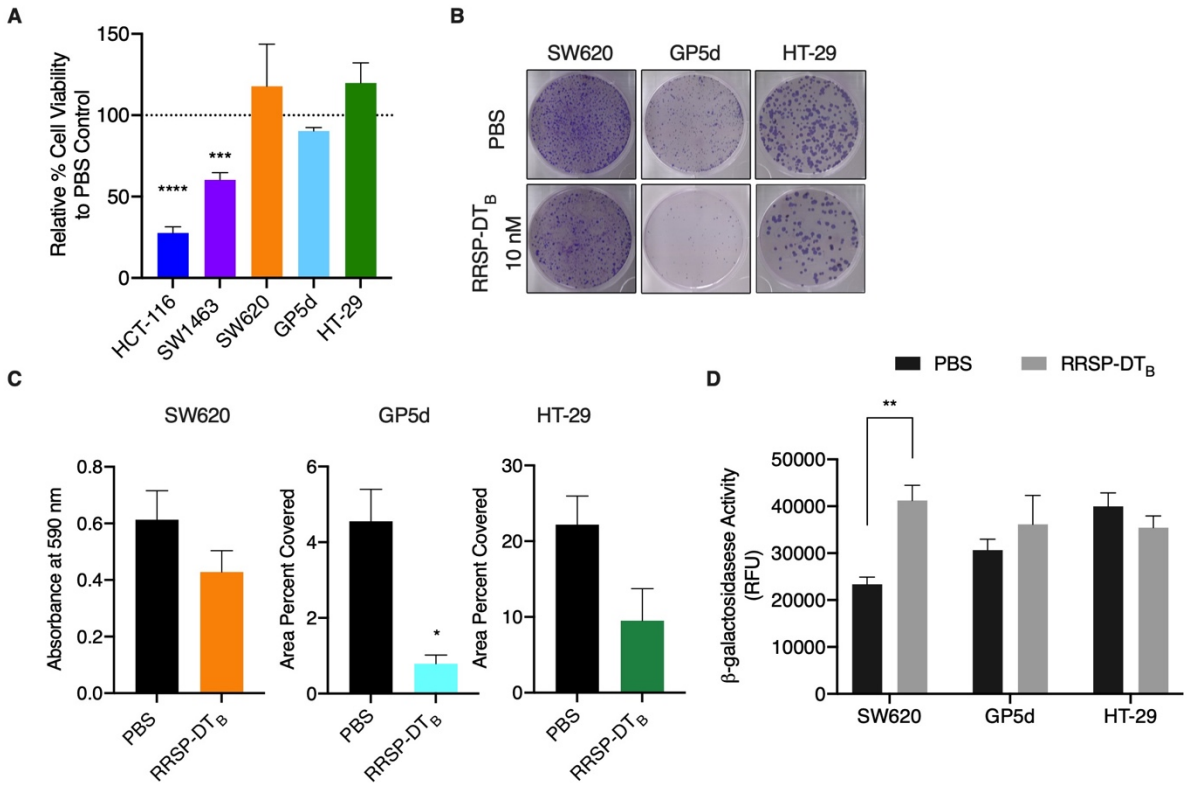

Figure 3. RRSP-DT_B decreases viability and causes irreversible growth inhibition in KRAS dependent and independent colon cancer cell lines. (**A**) Relative percent viability after 72-hour treatment with 10 nM RRSP-DT_B compared to PBS control in colon cancer cell lines. (**B**) Representative images of crystal violet-stained colonies from RRSP less sensitive cell lines pretreated with 10 nM RRSP-DT_B for 48 hours and replated at low seeding density to form colonies over 14 days. (**C**) Quantitative analysis of crystal-violet stained colonies from less sensitive RRSP cell lines from three independent experiments. Results are expressed as means ± SD of three independent experiments (**D**) Measured cell senescence activity in RRSP less sensitive cell lines treated with 10 nM RRSP-DT_B for 48 hours then incubated with SA-ß-Gal Substrate for 1 hour at 37ºC, *n* = 3. Results are expressed as mean ± SEM of three independent experiments (*P<0.05, **P<0.01, ****P<0.0001 versus PBS control as determined through one-way ANOVA followed by Dunnett's multiple comparison test).

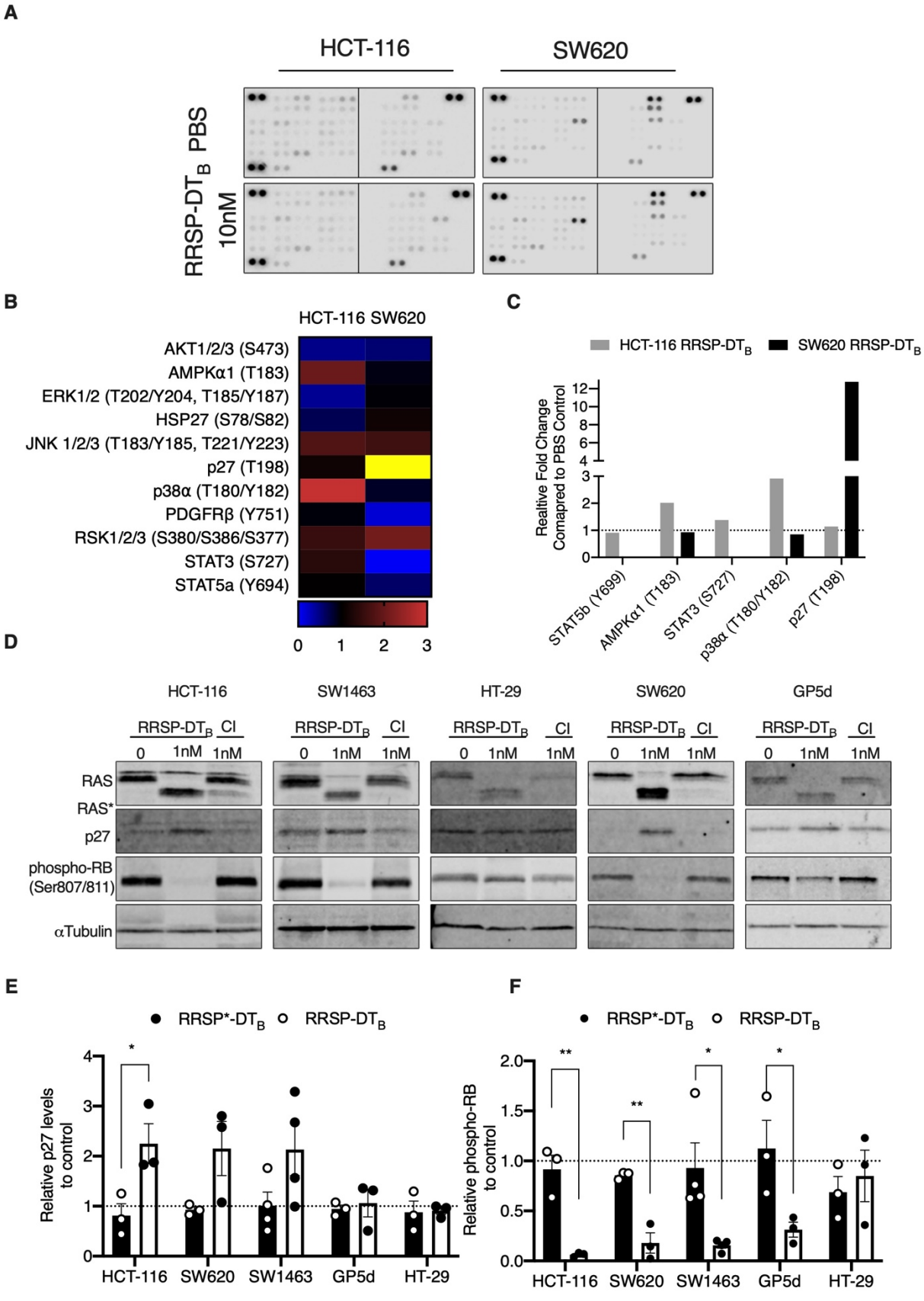

Figure 4. RRSP-DT_B cleavage of RAS induces p27 expression in colon cancer cell lines. (**A**) Human phospho-kinase array blots of HCT-116 and SW620 cells treated with either PBS or RRSP-DT_B (10nM) for 24 hours. (**B**) Densitometric analysis kinase array depicted through a heatmap of relative phosphorylated proteins levels in response to RRSP-DT_B compared to PBS control in HCT-116 and SW620 cells, *n* = 1. (**C**) Densitometric analysis phosphorylated proteins with largest differential phosphorylated protein levels between HCT-116 and SW620 treated cell lines, n=1. (**D**) Representative western blot images of p27 and phosphor-RB expression in colon cancer cell lines treated with either RRSP-DT_B or RRSP*-DT_B for 24 hours. (**E** and **F**) Densitometric analysis of fold change in p27 and phospho-RB compared to PBS after 24 hr in RRSP-DT_B treated colon cancer cell lines; *n* = 3. αTubulin was used as gel loading control. Results are expressed as mean ± SEM of three independent experiments (*P < 0.05, ** < 0.01, **** < 0.0001 versus PBS control as determined through one-way ANOVA followed by Dunnett's multiple comparison test).

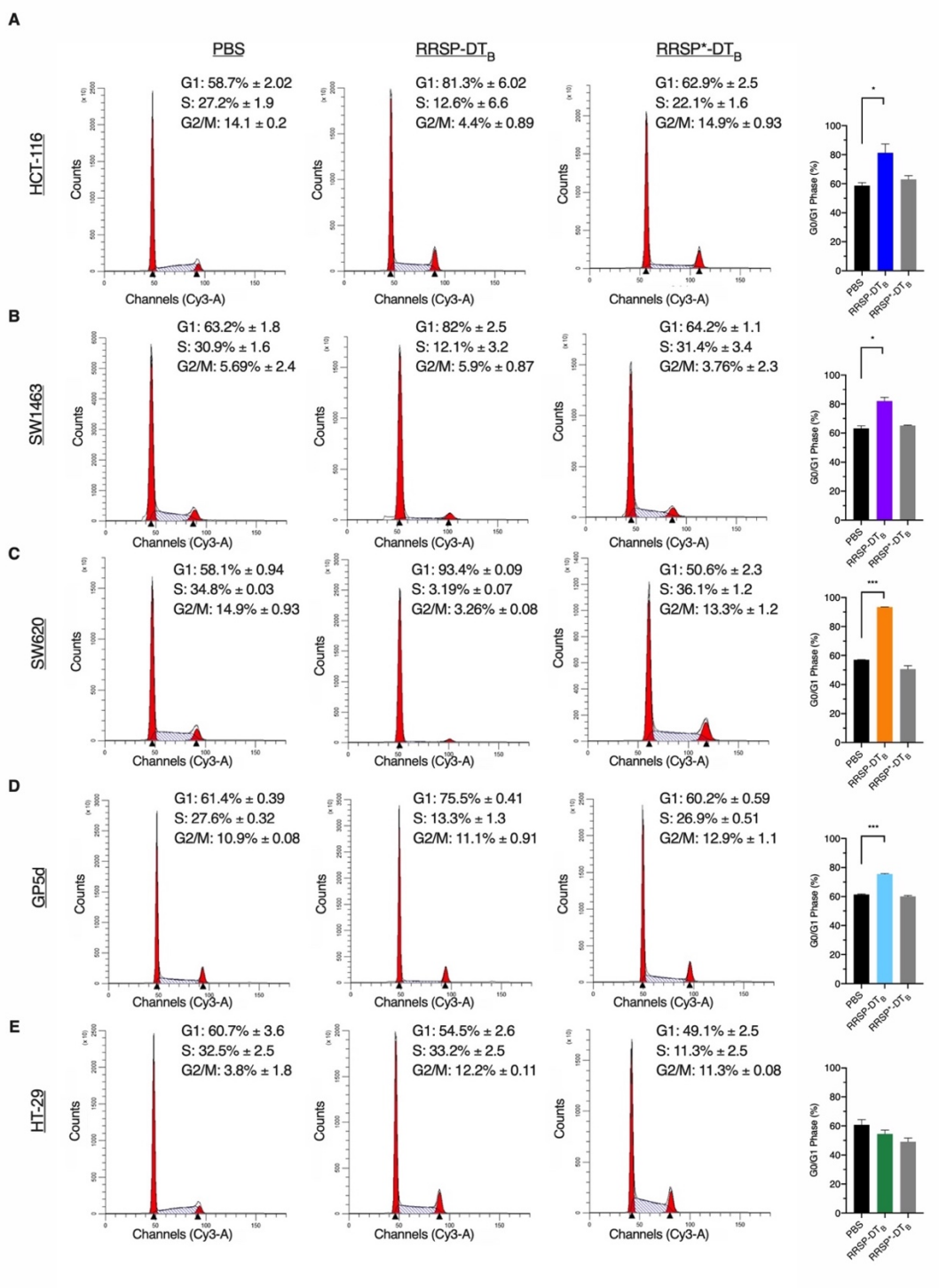

Figure 5. RRSP-DT_B induce G1 cell cycle arrest in colon cancer cell lines. (**A**-**D**) Cell cycle flow cytometry analysis of colon cancer cell lines treated with either PBS, RRSP-DT_B or RRSP*-DT_B (1nM) for 24 hours. Bar graphs depict percentage of cells in G1 phase for each treated sample; *n* = 3. Results are expressed as mean ± SEM of three independent experiments (*P<0.05, **P<0.01, ****P<0.0001 versus PA control as determined through one-way ANOVA followed by Dunnett's multiple comparison test).

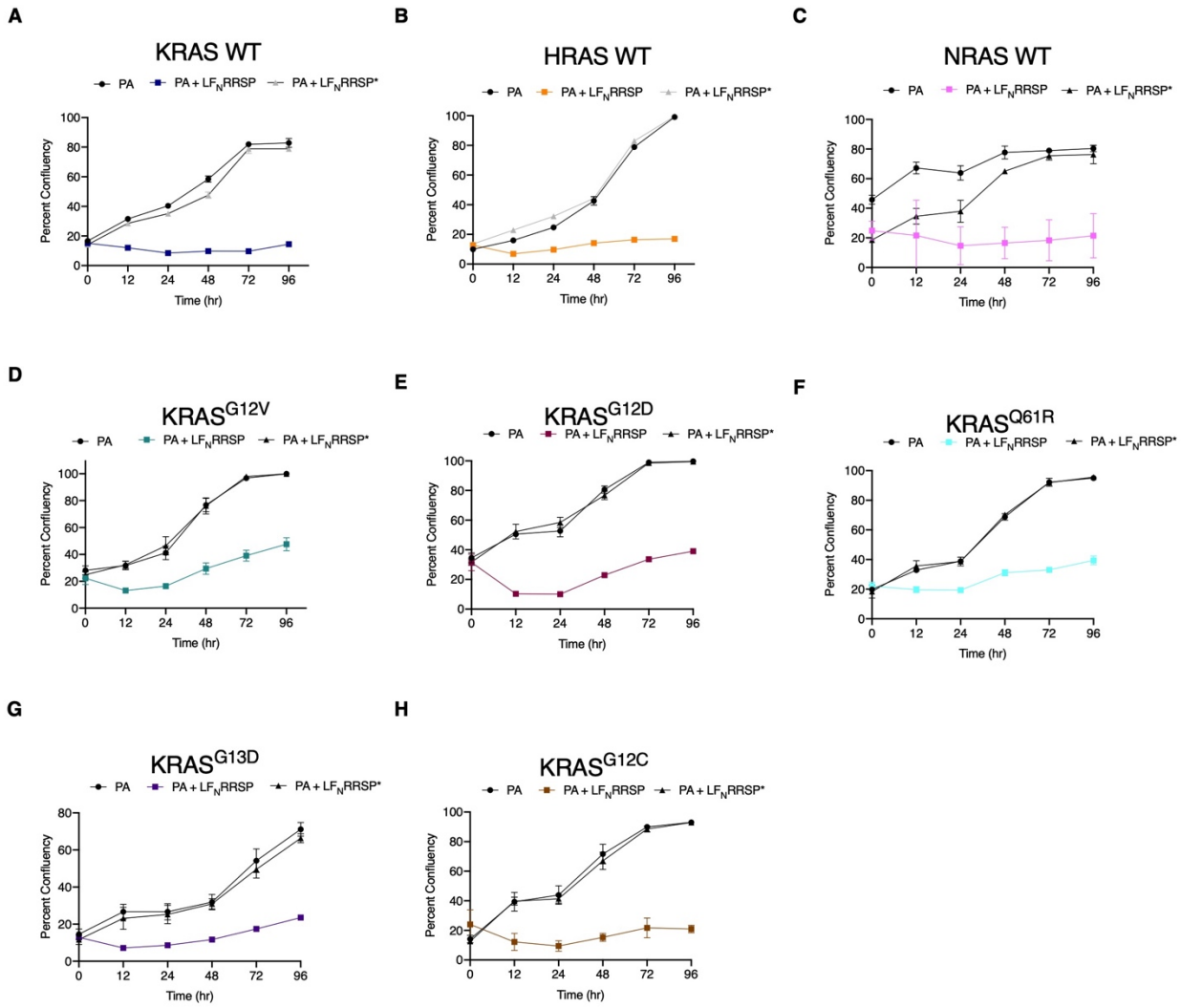

Supplementary Figure 1. Growth inhibition of RAS-less MEFs cell lines. (**A**-**H**) Growth inhibition observed in of RAS-less MEF cell lines at indicted timepoints following treatment with PA alone or in combination with LF_NRRSP or LF_NRRSP*; *n* = 3. Results are expressed as ± SEM.

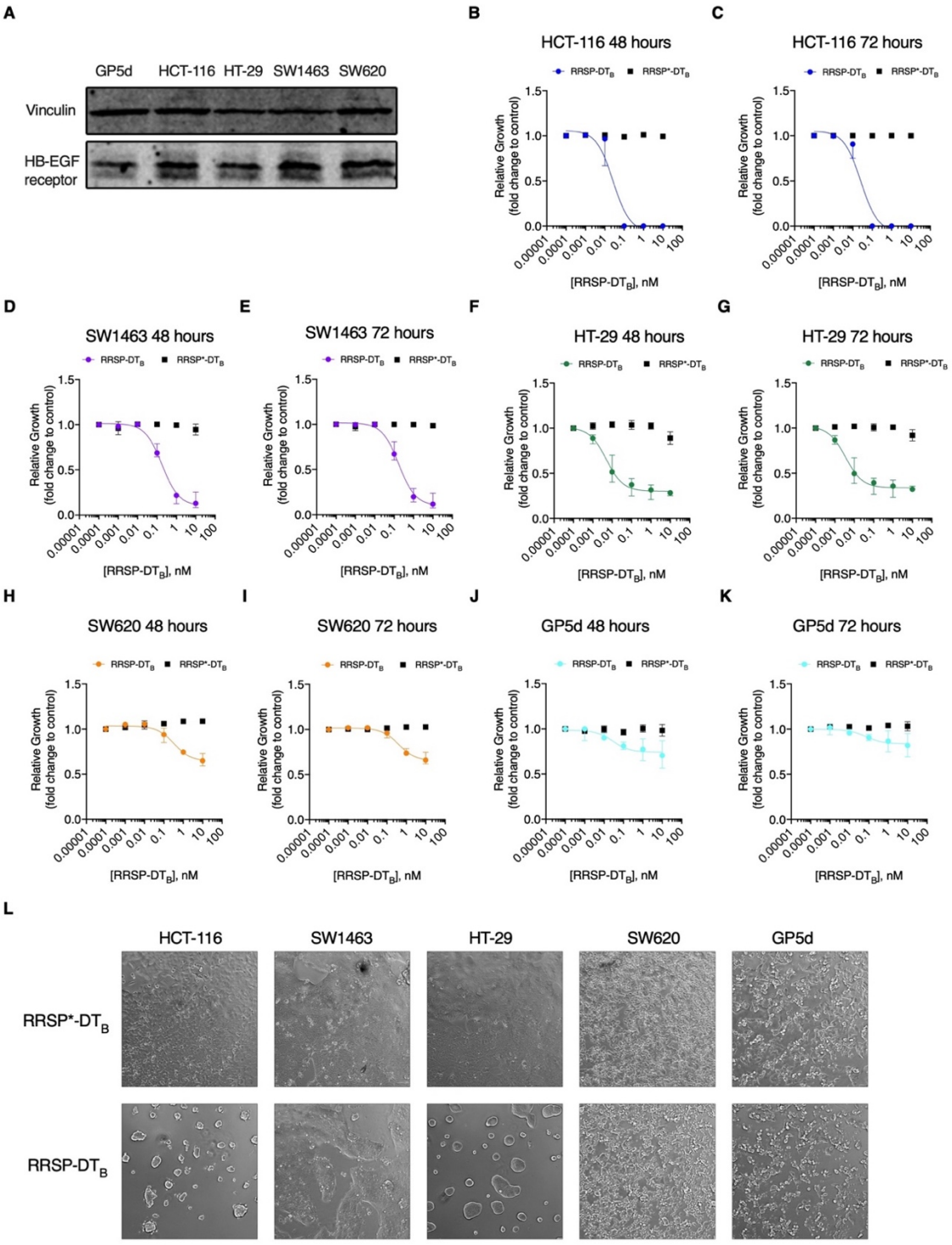

Supplementary Figure 2. Growth inhibition in RRSP-DT_B treated colon cancer cell lines. (**A**). Western blot analysis of HB-EGF receptor (DT receptor) from untreated colon cancer cell line lysates. Vinculin was used as loading control. (**B**-**K**) Fitted dose response curve of RRSP-DT_B in colon cancer cell lines after 48 and 72 hours. Results are displayed as mean ± SEM, *n* = 4. (**L**) Representative brightfield images of colon cancer cell lines treated with either RRSP-DT_B or RRSP*-DT_B (0.1 nM) after 24 hours.

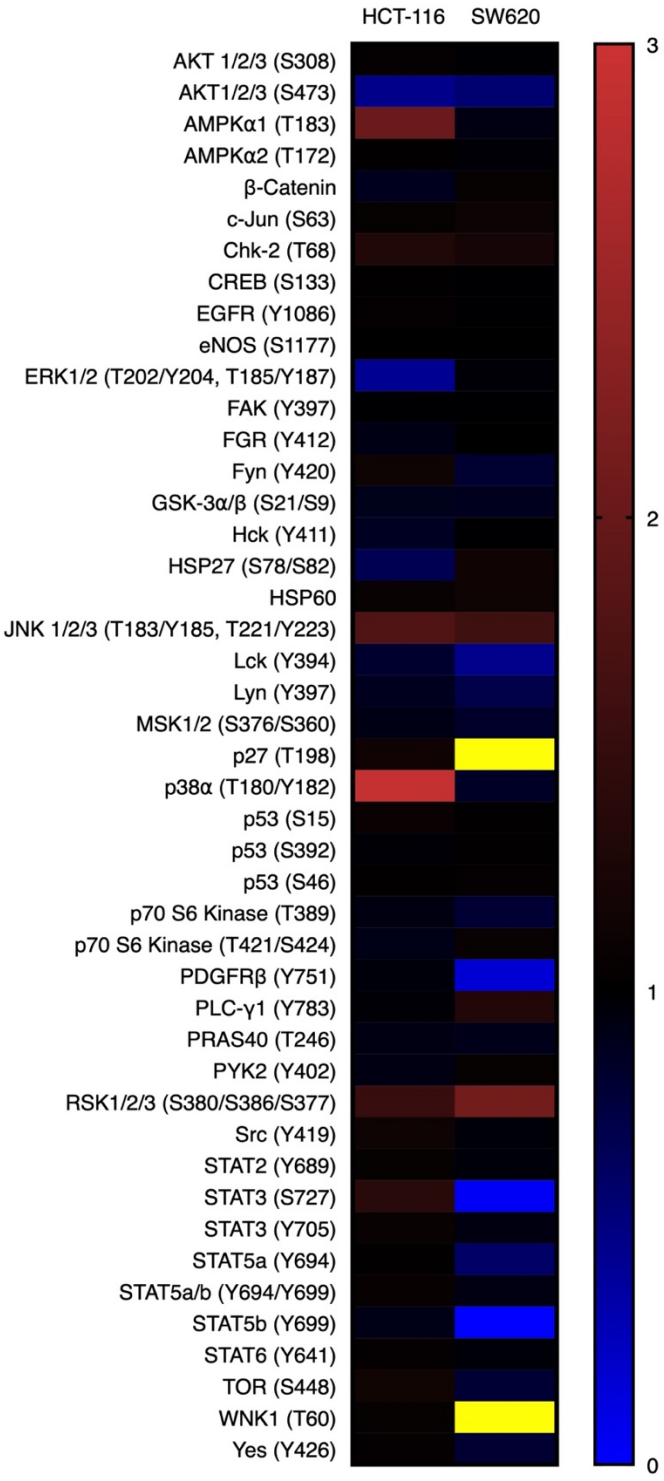

Supplementary Figure 3. Heatmap of human phosphor-kinase array in HCT-116 and SW620 cells treated RRSP-DT_B treated samples. Densitometric analysis of phospho-kinase array depicted through a heatmap of relative phosphorylated proteins levels in response to 10 nM RRSP-DT_B compared to PBS control in HCT-116 and SW620 cells after 24 hr.

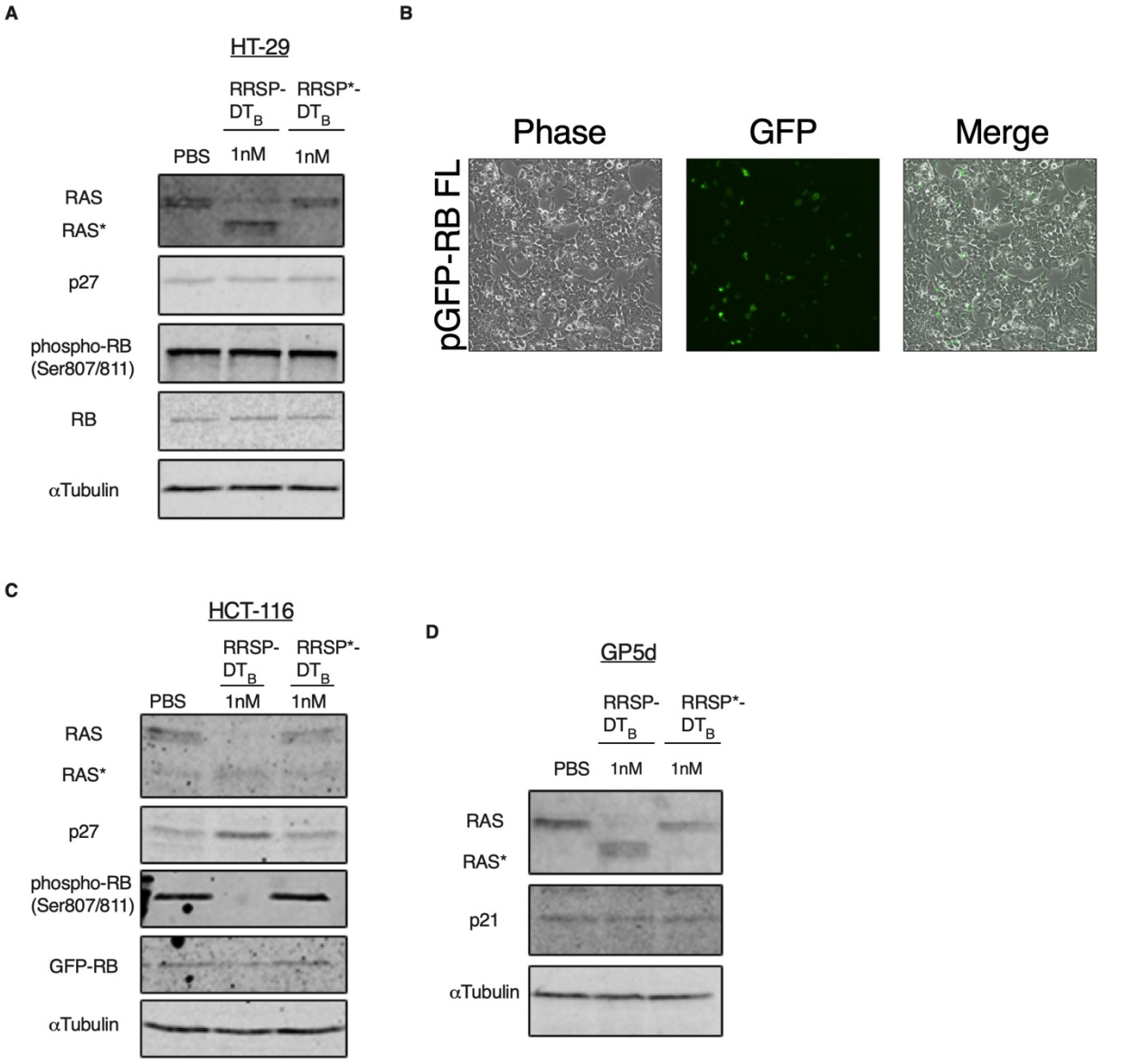

Supplementary Figure 4. Total RB expression in colon cancer cell lines. (**A**) Western blot analysis of endogenous total RB levels in HT-29 cells following treatment with either PBs, RRSP-DT_B or RRSP*-DT_B after 24 hr. (**B**) Representative images of HCT-116 cells transfected with pGFP-RB after 24 hr. (**C**) Western blot analysis of HCT-116 cells transfected with GFP tagged RB following treatment with either PBS, RRSP-DT_B or RRSP*-DT_B after 24 hours. Total RB was detected using anti-GFP primary antibody. αTubulin was used as a gel loading control (**C**) Western blot analysis of p21 levels in Gp5d cell treated with either PBS, RRSP-DT_B or RRSP*-DT_B after 24 hr.

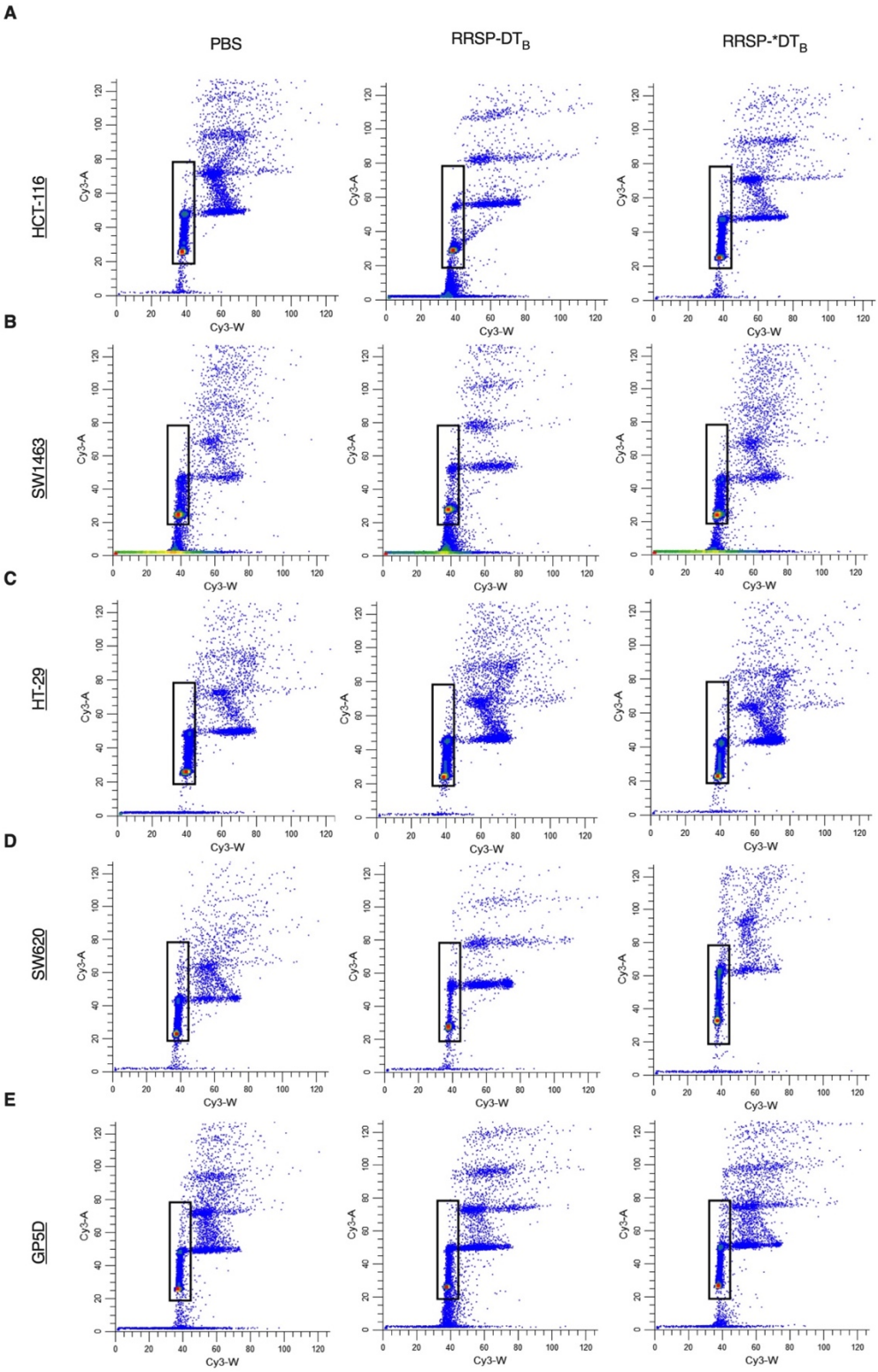

Supplementary Figure 5. Cell cycle analysis of colon cancer cell lines treated RRSP-DT$_B$. (**A**-**E**) Representative flow cytometry plots of colon cancer cell lines treated with either PBS, RRSP-DT$_B$ or RRSP*-DT$_B$ (1 nM) after 24 hours. Gating parameters were used to only collect single live cell populations.

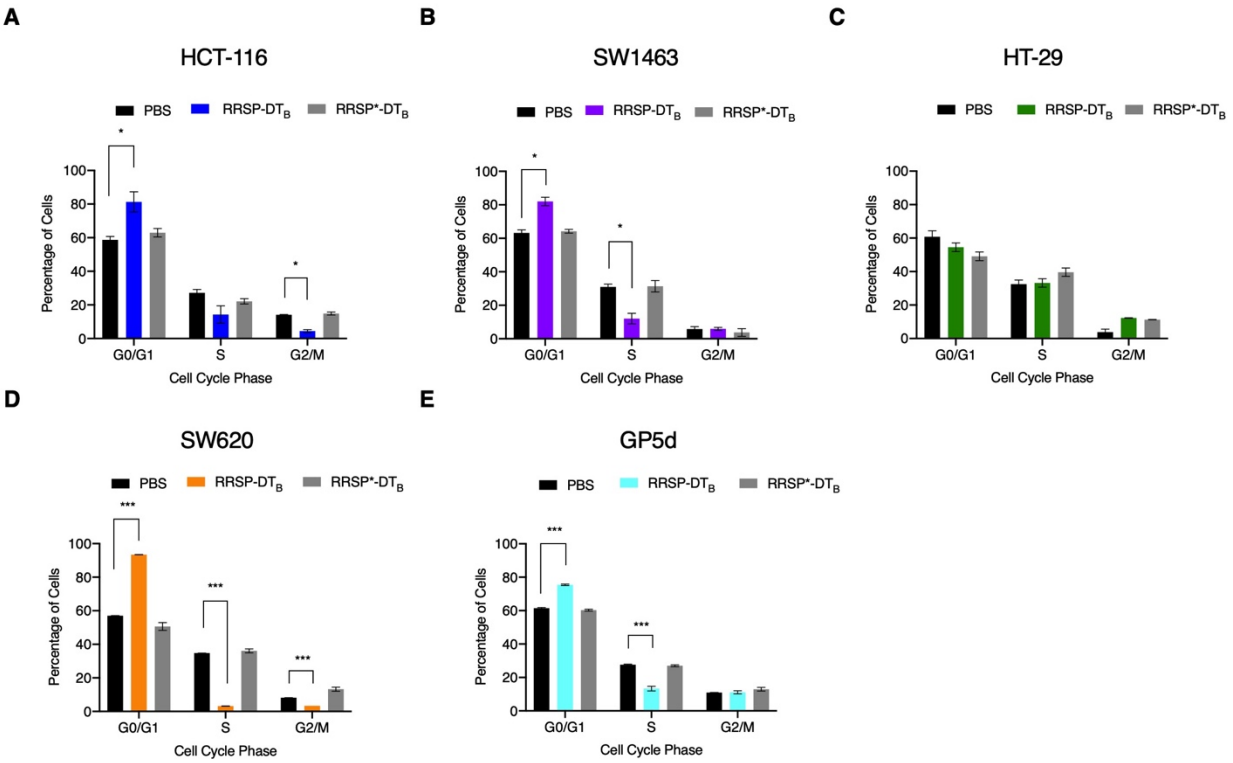

Supplementary Figure 6. Cell cycle analysis of RRSP-DT_B treated colon cancer cell lines. (**A**-**E**) Quantitative analysis of cell cycle analysis of colon cancer cell lines treated with PBS, 1 nM RRSP-DT_B or 1 nM RRSP*-DT_B for 24 hours; *n* = 3. Results are expressed as means ± SEM of three independent experiments (*P< 0.05, **P<0.01, ****P<0.0001 versus PA control as determined through one-way ANOVA followed by Dunnett's multiple comparison test).